Journal of Power Sources 630 (2025) 236119

Contents lists available at ScienceDirect

Journal of Power Sources

journal homepage: www.elsevier.com/locate/jpowsour

Direct electrolytic extraction of lithium metal from brines based on sandwich-structured garnet electrolyte

Nan Zhang [a,1], Hongpeng Zheng [a,1], Guoyao Li [a], Cheng Ouyang [a], Yu Yang [b], Hong Zhu [b], Rongzi Zhang [c], Haidong Sun [c], Chenglan Zhang [c], Hezhou Liu [a], Huanan Duan [a,*]

[a] State Key Laboratory of Metal Matrix Composites, School of Materials Science and Engineering, Shanghai Jiao Tong University, Shanghai, 200240, PR China
[b] University of Michigan-Shanghai Jiao Tong University Joint Institute, Shanghai Jiao Tong University, Shanghai, 200240, PR China
[c] QingHai Salt Lake Industry Co., Ltd., No. 28, Huanghe Road, Golmud, 816000, Qinghai, PR China

HIGHLIGHTS

- A sandwich-structured garnet was prepared to enable continuous Li extraction.
- The $La_2Zr_2O_7$ phase endows the pellet with unprecedented water stability.
- Li extraction rate can reach 126 μg cm^{-2} h^{-1} with current efficiency of 97.71 %.

ABSTRACT

Lithium metal is an important strategic resource with diverse industrial applications such as glass, ceramics, and alloys. With the increasing demand for lithium, lithium extraction from brines has become the focus of attention. However, due to the similarity of the radii of Li^+ and Mg^{2+}, conventional lithium extraction methods are inefficient for lithium extraction from brines with a high Mg/Li ratio. Herein we propose a direct electrolytic extraction of lithium (DEEL) system based on a sandwich-structured LLZTO ($Li_{6.5}La_3Zr_{1.5}Ta_{0.5}O_{12}$) electrolyte with excellent water stability. The lanthanum zirconate ($La_2Zr_2O_7$) on the surface of this sandwich-structured LLZTO can achieve high stability to water and air while still maintaining high ionic conductivity (7.5×10^{-4} S cm^{-1}) and low lithium interface resistance (40 Ω cm^2). This sandwich-structured LLZTO has been successfully demonstrated to stably extract lithium from simulated and natural brines. The current density for lithium extraction can reach 0.5 mA cm^{-2}, corresponding to a lithium extraction rate of 126 μg cm^{-2} h^{-1}; the electrochemical extraction devices can stably work for 48 h; the current efficiency can reach 97.71 %. The extracted lithium metal exhibits a purity of 99.475 wt%. This work provides a highly efficient approach for extracting lithium from brines by electrolysis.

1. Introduction

Lithium metal has attracted enormous attention due to its growing applications in light alloys, electronic equipment, electric vehicles, and power grid energy storage. One major thrust in developing next-generation lithium-ion batteries, e.g., all-solid-state lithium batteries, Li-S and Li-air batteries, is to use lithium metal anode because of its low electrode potential (−3.05 V vs. H_2/H^+) and high theoretical specific capacity (3860 mAh g^{-1}) [1–3]. However, with the growing demand for lithium in recent years, the sustainability of lithium resources has gained more attention than ever. It is estimated that a total of 5.11 million tons of lithium will be consumed by 2050 [4,5]. On the supply side, the lithium resources mainly exist in solid phases like ores and aqueous phases like salt-lake brine and seawater; the former is limited (about 10 %), unevenly distributed, and inefficient to extract from Ref. [6] and the latter has a large reserve (about 90 %) and become promising to solve the problem of lithium shortage [7,8].

Up to the present, various methods have been developed to extract lithium in the form of lithium salts from aqueous resources, which include chemical precipitation [9], evaporation crystallization [10], solution extraction [11,12], ion exchange adsorption [13–15], electrodialysis [16,17], etc. Their pros and cons are summarized in Table S1. One common method for extracting lithium from waste lithium batteries is through leaching [18], but the product is usually Li_2CO_3. The use of clean energy such as solar energy for lithium extraction is an environmentally friendly and suitable method for large-scale production [19,20], but the product is usually LiOH rather than metallic lithium. For the production of metallic lithium, electrolysis of the lithium salt of LiCl in

* Corresponding author.
E-mail address: hd1@sjtu.edu.cn (H. Duan).
[1] Nan Zhang and Hongpeng Zheng contributed equally to this work.

https://doi.org/10.1016/j.jpowsour.2024.236119
Received 12 September 2024; Received in revised form 18 November 2024; Accepted 23 December 2024
Available online 30 December 2024

the molten state is usually employed, which consumes massive amounts of energy and produces noxious chlorine gas. This severely affects the sustainable production and use of Li. In this regard, it is highly desirable to develop an efficient method to directly extract lithium from salt-lake brine with low lithium content (0.01–0.6 wt%) and high Mg/Li ratio (>6) [21]. In fact, because of the similar physicochemical properties and close radii of Mg^{2+} and Li^{+} (72 p.m. for Mg^{2+}, 76 p.m. for Li^{+}), a simple chemical precipitation method will lead to excessive lithium loss [22].

In recent years, electrolysis based on solid electrolytes has been proposed for lithium extraction from brines [22,23]. Under the action of an electric field, Li^{+} ions in the brine are screened by the solid electrolyte and deposited on an inert cathode. At the same time, Cl^{-} and OH^{-} lose electrons on the anode surface to generate Cl_2 and O_2 gases, respectively. The lithium extraction rate of such electrochemical devices reaches 50 μg cm^{-2} h^{-1}, which is about three orders of magnitudes higher than conventional technologies such as ion exchange adsorption [13,14]. The solid electrolyte used in this technology must have high ion selectivity [24], high lithium-ion conductivity, good water resistance, and stability to lithium. Compared with other solid electrolytes, garnet-type solid electrolyte ($Li_7La_3Zr_2O_{12}$, LLZO) is more promising for lithium resource extraction thanks to its decent ionic conductivity (10^{-4} S cm^{-1}), good stability to lithium, wide electrochemical window (>5V) and a high lithium-ion transference number (close to 1) [25–27].

However, previous studies suggest that LLZO has poor water stability, as Yuta Shimonishi et al. [28] found that the grain boundary conductivity of LLZO immersed in 1 mol L^{-1} LiOH was significantly reduced because of the accumulation of decomposition products with high resistance. Xia et al. [29] demonstrated that LLZO undergoes Li^{+}/H^{+} exchange in contact with water, generating $LiOH{\cdot}H_2O$ on the surface of LLZO that cannot conduct Li^{+}. As a result, when Zhao et al. tried to employ LLZO for lithium extraction from brines, they had to use spark plasma sintering (SPS) to synthesize LLZO with a relative density of 99.2 % to improve the water stability and the extraction duration was merely 1 h [23]. Recently, Zheng et al. [30] proposed a solvent-free route based on a conventional solid-state reaction to prepare $Li_{6.5}La_3Zr_{1.5}Ta_{0.5}O_{12}$ (LLZTO) pellets with ultrahigh moisture stability, which is featured with high relative density, few grain boundaries, water-stable secondary phase of $La_2Zr_2O_7$ (LZO), and the Li^{+}-deficient garnet lattice. It is of high interest to explore this type of electrolyte to enable lithium extraction for a prolonged time.

Herein we design a direct electrolytic extraction of lithium (DEEL) system based on a sandwich-structured LLZTO electrolyte with excellent water stability that is fabricated using a modified solvent-free solid-state reaction route. The lithium-deficient components on both sides, LZO, result from natural degradation during sintering which can provide water stability while hardly affecting the lithium interface resistance (40 Ω cm^2); the LLZTO in the middle maintains a high ion conductivity (7.5×10^{-4} S cm^{-1}). After immersing the sandwich-structured LLZTO in deionized water for two weeks, the pH of the water only increased to 9.8. The garnet electrolyte with excellent water stability enables stable electrolytic operation for 48 h, achieves a maximum lithium extraction rate of 126 μg cm^{-2} h^{-1}, and produces electrolytic lithium with a purity over 99 wt% in a simulated brine with a Mg/Li ratio of 10.

2. Results

2.1. DEEL system design and construction

As schematically shown in Fig. 1, the proposed DEEL system includes the following three main steps: preparation of garnet electrolyte, electrolytic lithium extraction, and post-treatment of the brine (removal of Cu^{2+} by adsorption). It, compared to conventional methods in Table S1, possesses the following features: 1) it greatly simplifies the multi-step process in traditional lithium extraction techniques, such as lithium-ion enrichment, separation of impurity ions, and lithium salt precipitation, and avoids the use of toxic reagents; 2) unlike traditional processes where the product is lithium salts, this technology is expected to achieve efficient direct extraction of metallic lithium and "produce lithium in one step"; 3) renewable energy sources such as solar energy could be used as the energy input of the system; 4) since brine lithium sources are often distributed in areas rich in wind and solar resources, this technology is conducive to the cross-regional transfer of renewable

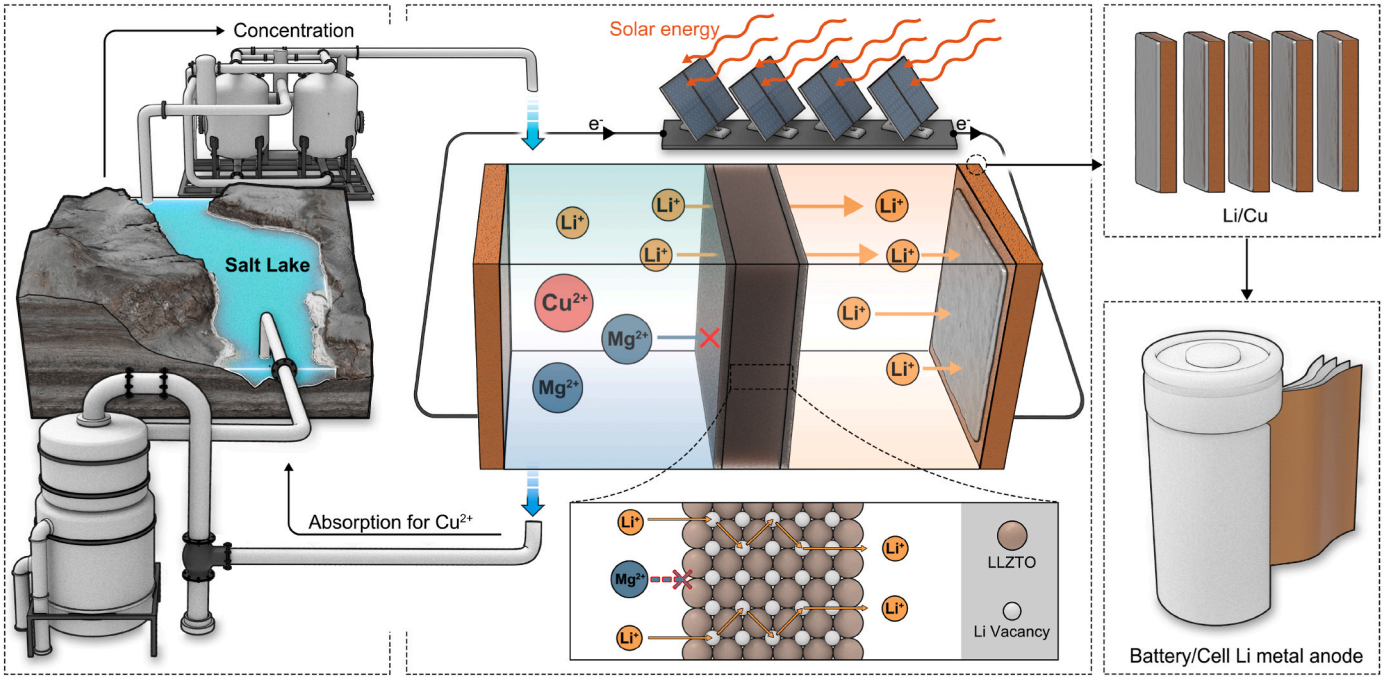

Fig. 1. | Schematic illustration of the DEEL system with a Li-free configuration and a sacrificial anode. The DEEL process includes preparation of garnet membrane electrolytic lithium extraction and post-treatment of the brine. The electric energy input can come from renewable sources such as solar energy, and the final outputs are high-purity lithium metal that can be used as anode for lithium batteries.

energy.

The working mechanism of the DEEL cell is depicted in the insert of Fig. 1. The garnet electrolyte separates the cathode and anode parts. On the cathode where lithium metal is deposited during the cell operation, lithium can wet the electrolyte to make a Li/garnet configuration, or liquid organic electrolyte (LOE) with a polymeric separator can be used to make a Li-free configuration. On the anode side, the garnet electrolyte directly meets brines and a complementary anode is needed to complete the cell. Renewable energy resources such as solar panels can be used to power the cell. During electrolysis, cations in the brine (Li^+, Mg^{2+}, etc) are driven by the electric field to move from the aqueous solution toward the lithium-ion-selective membrane, i.e., the garnet electrolyte. Due to the good selectivity of the garnet membrane [25,31], only lithium ions transport through the membrane and get reduced in the cathode compartment and the other cations are blocked and remain in the brine. Meanwhile, Cl^- and OH^- lose electrons on the anode surface to generate Cl_2 and O_2 gases, respectively, if an inert anode is used; or the gas evolution can be avoided if a sacrificial anode is used. The dissolved Cu^{2+} needs to be recovered by, for instance, absorption before the post-extraction brine is discharged back to nature.

As shown in Fig. S1a, the main components of a demonstration device include a stainless-steel connector, wedge-shaped polytetrafluoroethylene collar, stainless-steel spring and gasket, upper and lower rubber sealing rings, upper and lower housings, screws, bolts, and nuts for tightening. The device mainly relies on the pressure between the upper and lower housings to extrude the sealing rings for deformation,

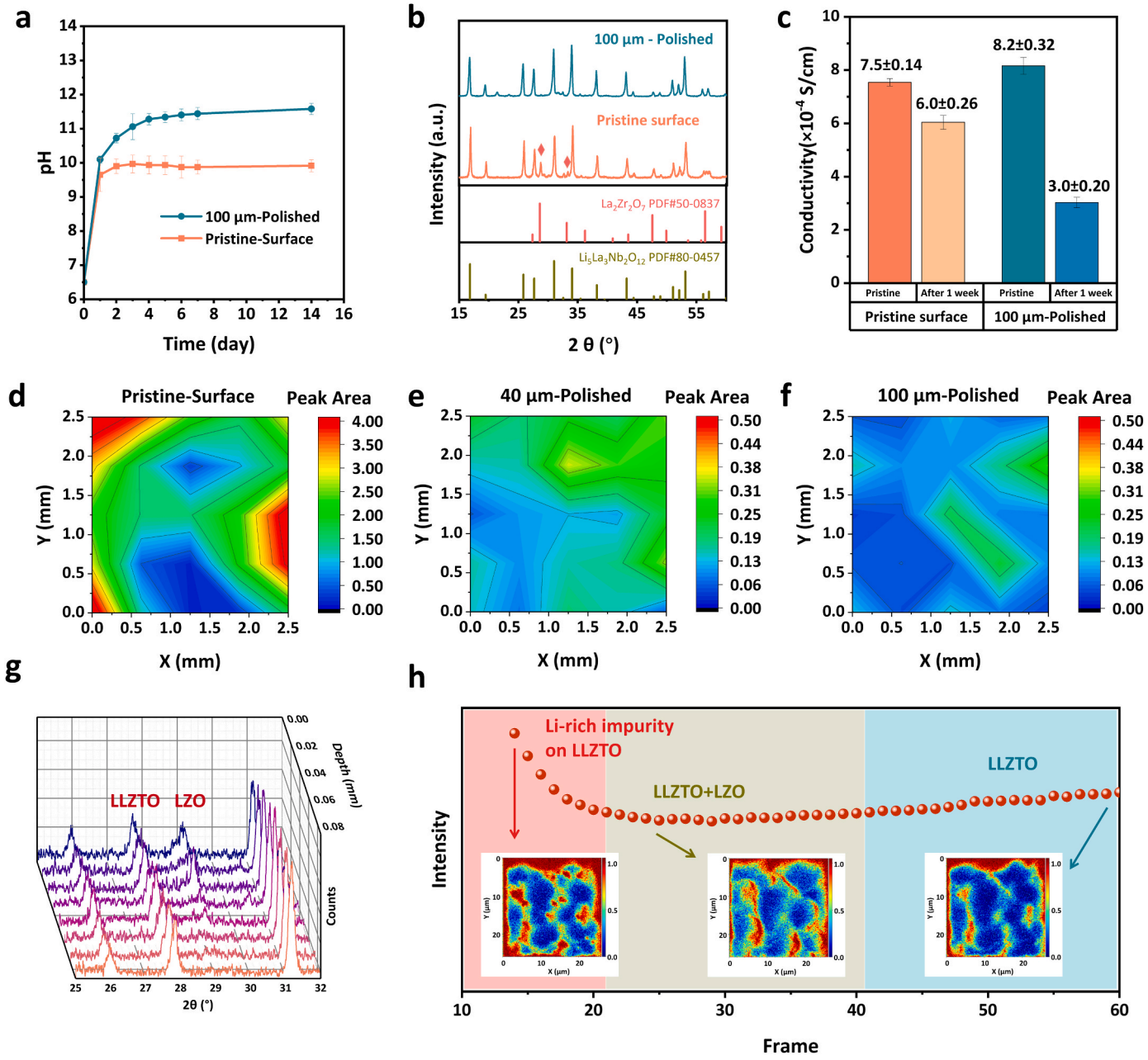

Fig. 2. | Materials characterization of the water-stable sandwich-structured LLZTO. a, The pH changes of LLZTO after immersion in deionized water for 14 days. **b**, The XRD patterns of LLZTO pellets after immersion in deionized water for 14 days. **c**, The ionic conductivity comparison before and after immersion in deionized water for 7 days. **d-f**, Integral 2D distribution of specific diffraction peaks for the (**d**) Pristine-Surface, (**e**) 40 μm-Polished surface, and (**f**) 100 μm-Polished surface. The value on the right is the ratio of the peak areas of LZO (29.1°) and LLZTO (27.8°). **g**, Waterfall XRD patterns of the cross-section of the sandwich-structured LLZTO at different depths. **h**, TOF-SIMS test result of the sandwich-structured LLZTO.

to achieve the sealing effect, and to avoid the corrosion of brine and air with lithium on the cathode side. The actual setup is shown in Figs. S1b and c. The effective contact area between LLZTO and brine is 1 cm^2, and the thickness of the LLZTO pellet is 1.5–2 mm.

2.2. Materials characterization of the sandwich-structured LLZTO

To apply the LLZTO membrane in the DEEL system, it is of paramount importance to verify the long-term stability in water. A water immersion test was carried out for the as-prepared and polished LLZTO pellets (Fig. S2). Here, the "Pristine-Surface" is the initial unpolished surface; the "40 μm-Polished" and "100 μm-Polished" refer to the samples after 40 μm and 100 μm thick surfaces polished with sandpaper. The exchange between H^+ in deionized water and Li^+ in LLZTO results in a decrease in H^+ content and an increase in OH^- content in the water, leading to an increase in the pH of the deionized water. As shown in Fig. 2a, for the Pristine-Surface, the pH of the deionized water rises and reaches a plateau after one day, and the final stable pH was about 9.8. In contrast, for the 100 μm-Polished LLZTO, the pH of the deionized water is stabilized at about 11.6 after 7-day immersion. The corresponding concentration of the dissolved Li^+ is 6.5×10^{-5} and 3.98×10^{-3} mol L^{-1}, which proves that LLZTO before polishing has long-term stability to water. It is worth mentioning that the mass concentrations of the above two dissolved Li^+ are 0.44 mg L^{-1} (ppm) and 27.9 mg L^{-1} (ppm) respectively, while the concentration of Li^+ in salt-lake brines varies from tens to hundreds ppm [32,33]. This suggests that the dissolved lithium from the pristine LLZTO is negligible, implying potential application in lithium extraction from salt-lake brines. The XRD spectrum of LLZTO in Fig. 2b after immersing in water for 14 days shows almost no impurity peaks, indicating good chemical stability of pristine LLZTO in water. Impurity peaks associated with Li_2CO_3 are observed for the 100 μm-Polished LLZTO sample. After immersing in water for one week, the conductivity of unpolished LLZTO reduced from 7.5×10^{-4} (Fig. S3) to 6.0×10^{-4} S cm^{-1}, while the conductivity of polished LLZTO reduced from 8.2×10^{-4} (Fig. S3) to 3.0×10^{-4} S cm^{-1}, as shown in Fig. 2c. SEM images (Figs. S4 and S5) suggest that little change is observed on the cross-section images for the pristine LLZTO before and after the water immersion test; while for 100 μm-Polished LLZTO, an impurity layer forms on the pellet surface.

In addition, the stability of the polished and unpolished LLZTO in the air was tested. The Ag|LLZTO|Ag symmetric batteries were placed in the air for one week and the lithium-ion conductivity before and after one week was tested. The results are shown in Fig. S6. The conductivity of unpolished LLZTO reduced from 7.5×10^{-4} to 6.2×10^{-4} S cm^{-1}, while the conductivity of polished LLZTO reduced from 8.2×10^{-4} to 5.8×10^{-4} S cm^{-1}. The reduction rate is 17.3 % and 29.3 % respectively, proving that the unpolished LLZTO also has better stability in the air.

To explore the origin of the much-improved water stability of the as-prepared LLZTO pellets, the crystal structure was examined with XRD. The phase structures of Ta5Li-4, Ta5Li0, and Ta5Li4 samples are shown by XRD in Fig. S7. Fig. S7b shows that the Pristine-Surface of Ta5Li0 has only cubic garnet phase (PDF# 80–0457) and $La_2Zr_2O_7$ (PDF# 50–0837). This implies that controlling the lithium excess can reduce the lithium concentration on the surface of LLZTO and form a water-stable LZO phase. Fig. S7b also shows that the LZO content decreases when the top surface of the pellet is polished away. Specifically, the LZO content is less on the 40 μm-Polished surface than on the Pristine-Surface and this phase disappears on the 100 μm-Polished surface. A similar trend appears in Ta5Li-4 (Fig. S7a) and Ta5Li4 (Fig. S7c). LZO can still be detected on the 100 μm-Polished surface of Ta5Li-4, while Ta5Li4 has a pure cubic phase structure on the 40 μm-Polished surface. This is because the lithium content in Ta5Li4 is relatively high, so it will not generate many lithium deficient LZO phases. Ta5Li-4 with relatively low lithium content will generate LZO at deeper depths. By comparison, it can be found that the LZO content on the Pristine-Surface of Ta5Li0 is moderate, which can enhance the water stability of LLZTO without losing the lithium-ion conductivity. The Ta5Li0 pellet with relative density of 96.8 % (Table S2) and a diameter of 15.5 mm is composed of densely packed micron-sized grains. So we chose Ta5Li0 for further experimentation.

Furthermore, surface mapping and linear scanning of XRD were used to obtain statistical phase compositions of the Ta5Li0 pellet. For mapping, 5 × 5 points with an interval of 0.5 mm were examined on the Pristine-Surface, 40 μm-Polished, and 100 μm-Polished surfaces of the Ta5Li0 pellet. The ratio of the LZO peak area at 29.1° to the LLZTO peak area at 27.8° is shown in Fig. 2d–f. The red area with a larger ratio represents more LZO on the Pristine-Surface, while the blue area of the 40 μm-Polished and 100 μm-Polished surfaces gradually increases, meaning that the LZO content decreases with the increase of depth. Besides the distribution of LZO, the orientation of the LLZTO grains may also cause the uneven distribution because orientation of the grains may lead to an increase or decrease in the intensity of the characteristic peaks in XRD. Indeed, the orientation of the garnet grains was observed by other researchers [34]. Fig. 2g shows the XRD linear scanning results of the cross-section of the Ta5Li0 pellet. As the depth increases, the peak intensity of LZO gradually decreases and completely disappears at 80 μm, which is consistent with the results in Fig. S7. The results of TOF-SIMS are shown in Fig. 2h. An analysis crater size of 25 μm × 25 μm is used so that the information of both the grains and the grain boundaries can be collected, and verified by the morphology inspection in Fig. S8. As the depth gradually deepens, the signal intensity of the Li element first decreases and then increases. The areas with strong lithium element signals (red region) are associated with trace amounts of lithium-containing impurities (Li_2CO_3 and $LiOH{\cdot}H_2O$) formed on the surface of LLZTO pellet [35], which are too few to be characterized by XRD; the areas with weak signals (light green region) represent the lithium-deficient phase, H-LLZTO and LZO; the light blue region implies the pristine LLZTO bulk phase. It can be concluded from Fig. 2 and S7 that a sandwich structure can spontaneously form for the LLZTO pellet synthesized via the solvent-free solid-state reaction method.

The mechanism of the spontaneous formation of lithium-deficient layers during synthesis is explored through theoretical calculations, and the temperature at which LLZTO spontaneously loses Li_2O to form a lithium-deficient phase (Equation (1)) is determined. The results are shown in Table S3. At room temperature (300 K), the Gibbs free energy (ΔG) for the loss of Li_2O is 2.02 eV, a value greater than 0, which indicates that LLZTO will not spontaneously lose Li_2O at this temperature. As the temperature increases, ΔG gradually decreases. When the temperature reaches 1000–1100 K, the ΔG of the reaction is below 0, meaning that the reaction can proceed spontaneously. The sintering temperature in this study is 1320 °C (≈1600 K), and the reaction ΔG equals −2.23 eV, suggesting that LLZTO can spontaneously lose Li_2O and form a lithium-deficient phase during sintering. According to the previous research [30], the lithium-deficient LLZTO shows a more positive ΔG reacting with water compared to stoichiometric LLZTO, meaning that the lithium-deficient phase has less tendency to react with water and subsequently higher water stability than stoichiometric LLZTO. Furthermore, according to the calculation, after losing 7 Li_2O molecules, LLZTO undergoes lattice collapse and generates LZO as shown in Equations (2) and (3).

$$Li_{52}La_{24}Zr_{12}Ta_4O_{89} \rightarrow Li_{50}La_{24}Zr_{12}Ta_4O_{95} + Li_2O \quad (1)$$

$$Li_{52}La_{24}Zr_{12}Ta_4O_{89} \rightarrow Li_{38}La_{24}Zr_{12}Ta_4O_{89} + 7Li_2O \quad (2)$$

$$3Li_{38}La_{24}Zr_{12}Ta_4O_{89} \rightarrow 5La_2Zr_2O_7 + 31La_2O_3 + 12Li_3TaO_4 + 13Li_6Zr_2O_7 \quad (3)$$

2.3. Operation performance of the DEEL system

Here, we used a constant current power source as a consistent energy supply to study the lithium extraction performance of the DEEL system,

even though it could be replaced with clean energy sources such as solar energy in the future. We first tested the Li/garnet configuration with a sacrificial anode as shown in Fig. 3a. By spreading the molten lithium on LLZTO, we obtained an intimate Li|LLZTO interface as displayed in Fig. 3b. The Nyquist diagram of the Li|LLZTO|Li symmetric batteries is shown in Fig. 3c. The high-frequency and intermediate-frequency regions show a semicircle, and the low-frequency region shows a diffuse tail. The x-intercept of the semicircle in the high-frequency region can be attributed to the internal resistance of LLZTO, which is mainly the impedance formed by lithium-ion transfer at the lattice and grain boundary; the interface resistance (charge transfer resistance) can be determined by the diameter of the semicircle, and the tail of low frequency corresponds to the diffusion of lithium ions in the electrode. Table S4 shows the resistance of bulk, grain boundary (gb), and Li|LLZTO interface obtained through the equivalent circuit fitting in Fig. 3c. The interfacial area-specific resistance (ASR) can be obtained by multiplying the interface resistance by the area of the LLZTO pellet. The interfacial ASR of Li|Pristine-Surface|Li and Li|100 μm-Polished|Li symmetric cells is 40 Ω cm^2 and 28 Ω cm^2 respectively. Due to the presence of a small amount of LZO on the pristine surface, the interface resistance to lithium is slightly higher than that of the polished LLZTO pellet.

The lithium extraction performance of the DEEL system with the Li/garnet configuration is studied using a 1 mol L^{-1} LiCl solution as the simulated brine. During electrochemical lithium extraction, the electrochemical reactions are as follows:

$$Li^+ (aq) + e^- \rightarrow Li (s) \quad (4)$$

$$Cu (s) \rightarrow Cu^{2+} (aq) + 2e^- \quad (5)$$

On the cathode side, Li^+ at the Li|LLZTO interface is reduced to metallic lithium as Equation (4). The reaction of Cu as a sacrificial anode occurs as shown in Equation (5). The working electrode is the coated Li while the counter and reference electrode is the salt-lake side copper electrode.

As shown in Fig. 3d, the Li/garnet configuration has been successfully operated for lithium extraction at different current densities (0.02, 0.04, 0.06, 0.08, and 0.10 mA cm^{-2}) for 1 h. The cell voltage reaches a stable value within several minutes and the corresponding stabilized voltage is 2.92 V, 2.96 V, 3.02 V, 3.09 V, and 3.16 V respectively. This indicates that the lithium extraction rate can reach 26 μg cm^{-2} h^{-1}. The lithium extraction rate per square centimeter of LLZTO and per gram of LLZTO per hour is calculated using Equations (6) and (7):

$$\text{Quantity of electricity} : Q = I \times t = 0.1\ \text{mA} \times 3600\ \text{s} = 0.36\ \text{C}$$

$$\text{Quantity of electrons} : n = \frac{Q}{F} = \frac{0.36\ \text{C}}{96485\ \text{C mol}^{-1}} = 3.7 \times 10^{-6}\ \text{mol}$$

$$\text{Mass of Li} : m = M \times n = 7\text{g mol}^{-1} \times 3.7 \times 10^{-6}\ \text{mol} = 26\ \mu\text{g}$$

$$\text{Lithium extraction rate (per cm}^2\text{)} : \frac{26\ \mu\text{g}}{1\ \text{cm}^2\ \text{h}} = 26\ \mu\text{g cm}^{-2}\ \text{h}^{-1} \quad (6)$$

$$\text{Lithium extraction rate (per g)} : \frac{26\ \mu\text{g}}{2\ \text{g h}} = 13\ \mu\text{g g}^{-1}\ \text{h}^{-1} \quad (7)$$

where Q is the quantity of electricity, I is the current, t is time, n is the quantity of electrons, F is Faraday's constant, and M is the relative atomic mass of lithium.

To study the long-term performance, lithium extraction is carried out at a current density of 0.05 mA cm^{-2} for 10 h, as shown in Fig. 3e. With the extraction of lithium, the polarization voltage gradually increases,

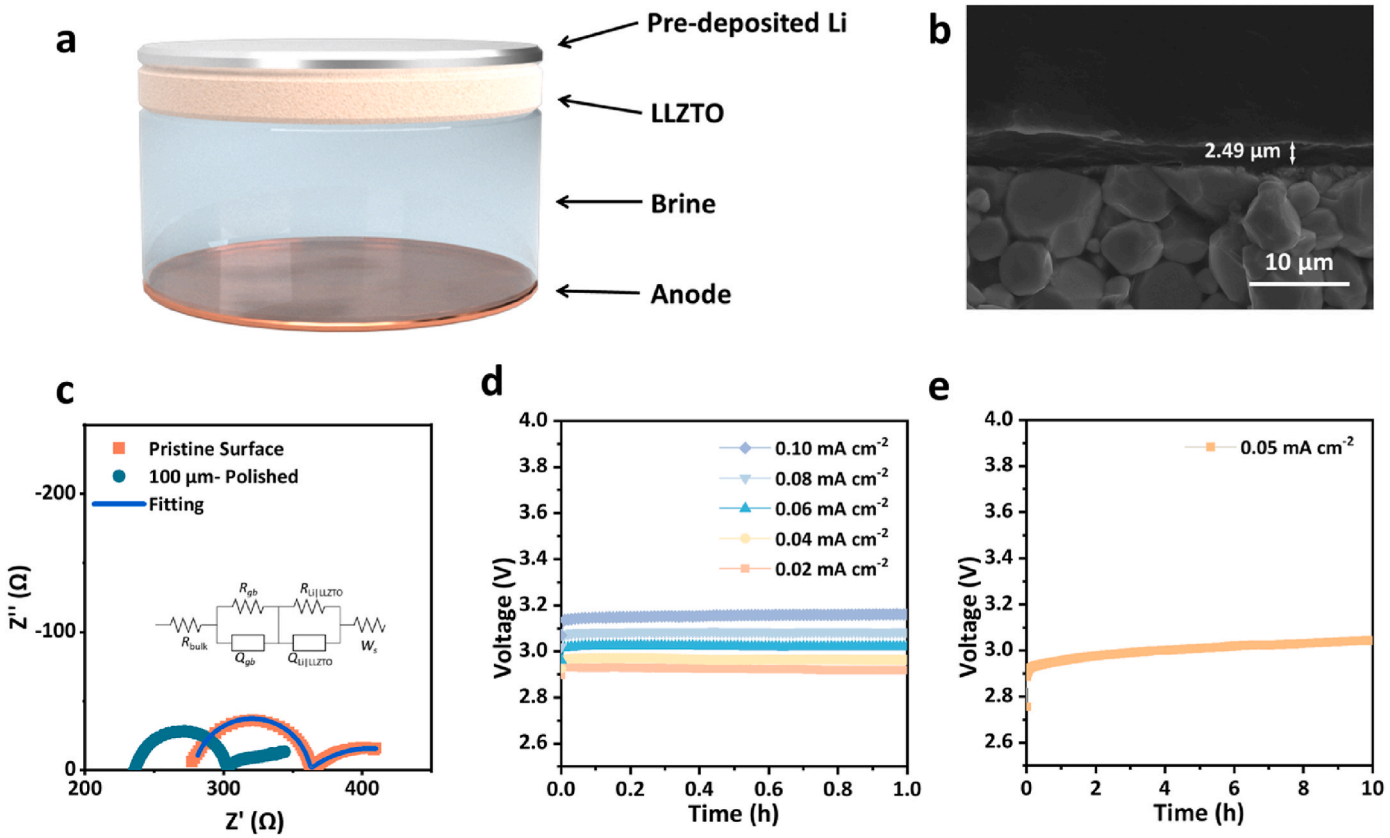

Fig. 3. | The lithium extraction performance of the DEEL device with a Li/garnet configuration. a, Schematic illustration of the device. **b**, SEM images of the Li|LLZTO metal interface. **c**, Li|LLZTO|Li EIS spectra comparison of Pristine-Surface and 100 μm-Polished surface, inset shows the equivalent circuit used for fitting. **d-e**, Operation performance with current densities of 0.02, 0.04, 0.06, 0.08, and 0.10 mA cm^{-2} for 1 h (**d**) and 0.05 mA cm^{-2} for 10 h (**e**).

which may be related to the concentration polarization at the LLZTO| brine interface. Fig. S9 shows the morphology of the Li|LLZTO cross-section after lithium extraction for 10 h with the current density of 0.05 mA cm^{-2}. From the results of line scanning, it can be seen that the thickness of Li metal extracted with a capacity of 0.5 mAh cm^{-2} is ~2.5 μm, which is consistent with the theoretical value [36].

We then tested the Li-free configuration as shown in Fig. 4a. This configuration can adapt to more extraction scenarios. The working electrode is the Li deposited on Cu while the counter and reference electrode is the salt-lake side copper electrode. Figs. S10 and S11 show the voltage curves of lithium extraction in different concentrations of LiCl simulated brine for 48 h at current densities of 0.10 and 0.20 mA cm^{-2}, demonstrating that LLZTO can stably extract lithium for a long time. Fig. 4b compiles the average cell voltage at different current densities from 0.10 to 0.50 mA cm^{-2} in simulated brines with Li^+ concentrations of 0.33, 0.6, and 1 mol L^{-1}. Obviously, there is a good linear relationship between the voltage platform and current density. The actual voltage profiles are depicted in Fig. S12. At a high current density of 0.50 mA cm^{-2}, the voltage platform remains stable below 4.8 V, implying that the chemical and electrochemical stability of the system ensures a stable lithium extraction process. It is noted that no evidence of the electrolysis of H_2O was observed during the lithium extraction process in Fig. 4b based on two phenomena: 1) no oxygen bubbles form on the counter electrode, 2) the current efficiency is about 97.71 % (Table S5), meaning few side reactions including H_2O decomposition. This can be rationalized as follows: at the potential of approximately 4.5V (Fig. S12c), the Li^+ ions in the brine migrate through the LLZTO membrane and get deposited on the Cu working electrode. The Cu/LOE interface, LOE, LOE/LLZTO interface, LLZTO, LLZTO/brine interface, and brine will withstand the majority of the potential drop, as a result, the potential on the counter electrode is not high enough to electrolyze the H_2O, similar to the aqueous rechargeable lithium battery using solid-electrolyte-protected Li metal as anode [37]. The corresponding lithium extraction rates are also shown in Fig. 4b, and a maximum lithium extraction rate of 126 μg cm^{-2} h^{-1} and 63 μg g^{-1} h^{-1} has been demonstrated.

As shown in Fig. 4c, when the Li^+ concentration was reduced to 0.01 mol L^{-1}, equivalent to the real salt-lake brine, the lithium extraction platform of the sandwich-structured LLZTO was still between 3.2 V and 4.4 V, indicating that the sandwich-structured LLZTO can be stably used in environments with different Li^+ concentrations and has little polarization effect. As shown in Fig. S13, LLZTO can still achieve 27 h of lithium extraction at a current density of 0.10 mA cm^{-2} in a LiCl solution with a concentration of 0.01 mol L^{-1}.

In order to study the ion selectivity of the sandwich-structured LLZTO, simulated brine with Mg/Li = 0 and 10 (molar ratio, C_{Li+} = 0.05 mol L^{-1}) was prepared for lithium extraction. As shown in Fig. 4d and Fig. S14, the voltage profiles at different current densities from 0.10 to 0.50 mA cm^{-2} are stable, proving that a Mg/Li ratio of 10 will not affect the lithium extraction performance of LLZTO. In addition, the cell has been successfully operated in both brines for 48 h. As shown in Fig. 4e, the voltage plateau is 3.23 V at a current density of 0.10 mA cm^{-2}. After the lithium extraction, the Cu current collector with the deposited Li was put into 15 mL ultrapure water, the Li^+ concentration in the water was measured through conducted inductively coupled plasma mass spectrometry (ICP-MS), and the current efficiency was

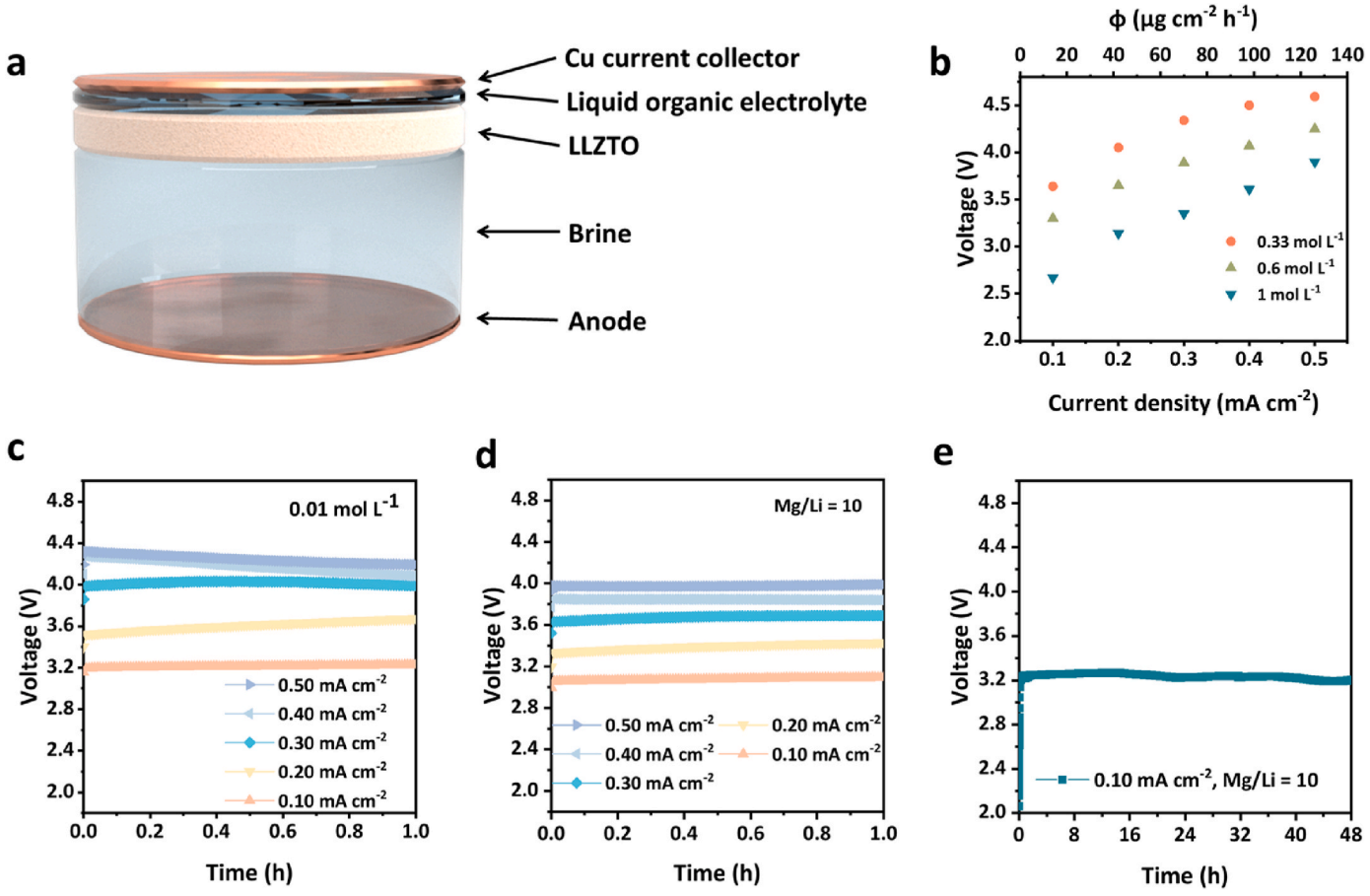

Fig. 4. | The lithium extraction performance of the DEEL device with a Li-free configuration. a, Schematic illustration of the device. **b**, Voltage platform and lithium extraction rate with current density of 0.10, 0.20, 0.30, 0.40, and 0.50 mA cm^{-2} in different concentrations of LiCl for 1 h **c**, Lithium extraction performance with current densities of 0.10, 0.20, 0.30, 0.40, and 0.50 mA cm^{-2} for 1 h. The LiCl concentration is 0.01 mol L^{-1}. **d-e**, Extraction in a solution of Mg/Li = 10 (mol:mol) with the current density of 0.10, 0.20, 0.30, 0.40, and 0.50 mA cm^{-2} for 1 h (**d**) and 0.10 mA cm^{-2} for 48 h (**e**).

calculated through Equation (8). As shown in Table S5, the current efficiency of lithium extraction in 0.05 mol L^{-1} LiCl with the Mg/Li ratio of 0 and 10 is 97.71 % and 86.74 %, respectively.

Fig. S15 shows the comparison of LLZTO surface morphology before and after lithium extraction in brine with Mg/Li = 10, and a small amount of impurity appears on the LLZTO|brine interface. XRD results shown in Fig. S16a prove that the composition of the impurity is $Mg(OH)_2$ (After-Brine); Meanwhile, no impurities were generated on the surface in contact with LOE (After-LOE), proving the stability of LLZTO in LOE. After lithium extraction, the lithium-ion conductivity of LLZTO decreased from 7.54×10^{-4} to 5.27×10^{-4} S cm^{-1} (Fig. S16b), still maintaining at a considerable level, and the water stability of LLZTO has been further testified.

In order to further investigate the lithium extraction performance of sandwich-structured LLZTO in LiCl solutions containing different impurity ions (Na^+, K^+, Mg^{2+}), LiCl solutions containing only one impurity ion were prepared according to the ratio in Table S6. The lithium extraction performance of sandwich-structured LLZTO in simulated mother liquor is shown in Fig. S17. At a current density of 0.10 mA cm^{-2}, the voltage platforms of K-simulated qualified solution and Na-simulated qualified solution are relatively stable. However, in the Mg-simulated qualified solution, there was an unstable voltage phenomenon after 30 h of lithium extraction. This can be explained by the generation of $Mg(OH)_2$ on the surface of LLZTO mentioned earlier. The $Mg(OH)_2$ impurity hinders the contact between LLZTO and the simulated qualified solution, causing an increase in polarization voltage.

Fig. S18 shows the lithium extraction performance of the sandwich-structured LLZTO in the brine from Chaerhan Salt Lake in Qinghai Province, China. The brine composition is shown in Table S7. The sandwich-structured LLZTO can stably extract lithium with a current density ranging from 0.05 to 0.08 mA cm^{-2}. The concentration of Li^+ and Mg^{2+} in the brine is determined through ICP-MS to be 335 mg L^{-1} and 1.5×10^5 mg L^{-1}, respectively, so the Mg/Li molar ratio is approximately 130. The ability to maintain a lithium extraction rate of 20 μg cm^{-2} h^{-1} in such a high Mg/Li environment demonstrates the promising application prospects of the sandwich-structured LLZTO in lithium extraction. On the one hand, the impurity ion of Mg^{2+} does affect the current efficiency, and more work is in progress to this end; on the other hand, this current efficiency is higher than other electrochemistry-based lithium extraction techniques (57.82 % [38], 65 % [39], and 79 % [23]).

Even though the Li/garnet configuration avoids using flammable organic electrolytes, it is difficult to achieve scale production due to the following presumable reasons. First, when using a large piece of garnet pellet, it is prone to cracking due to uneven thermal field distribution during the high-temperature Li-melting process. Second, the wetting step needs a considerable amount of molten Li. Third, the extracted Li is difficult to separate from ceramic pellets, which poses problems in cell disassembly and lithium characterization. On the other hand, using a Li-free configuration is beneficial for separating and analyzing extracted lithium metal, and holds a greater chance for scale application. Additionally, the Cu foil used in the Li-free configuration could be replaced with other scaffolds or lithium-free anode (e.g., Si-based anode) to do electrochemical prelithiation. A roll-to-roll prelithiation process has been proposed for such a purpose. The prelithiated anode via the DEEL system could be directly used for lithium-ion batteries [40]. Moreover, as shown in Table S8, the lithium extraction rate using the Li-free configuration is 5 times higher than that of the Li/garnet configuration thanks to the solid/liquid contact instead of the solid/solid contact in the latter, which means more efficient and faster lithium extraction. Because the uneven Li deposition (Fig. 3b) may cause loss of the solid/solid contact during Li extraction in the Li/garnet configuration, the cell voltage increases dramatically, exceeding the range that the equipment and LLZTO can withstand. In contrast, solid/liquid contact can ensure good contact and maintain a stable impedance during Li extraction. As a result, the current density and lithium extraction rate are larger for Li-free configuration than for Li/garnet configuration, as shown in Figs. 3d and 4b.

2.4. Characterization of the lithium product

The digital photo of the extracted lithium on Cu foil from the brine with Mg/Li = 10 is shown in Fig. 5a. The lithium deposition is uniform, showing a grayish-white color with a metallic luster. Through the SEM image, it can be seen that the morphology of lithium at the edge is uniformly arranged wormlike dendrites (Fig. 5b), while the dendrites in the center overlap and bond with each other, forming a porous structure (Fig. 5c). It is noted that as the extraction proceeds, Li dendrites may accumulate and penetrate the LLZTO membrane, limiting the areal capacity (thickness) of the deposited lithium. In the future, various strategies in Li metal battery such as using lithiophilic deposition substrates, using 3D scaffold to accommodate the volume change, artificial SEI engineering, etc. [41] might help increase the system's maximum production capacity. The XRD characterization of Cu foil after lithium deposition is shown in Fig. 5d. The peak at 36.2° is the characteristic peak of Li, while the other three are the characteristic peaks of Cu and no impurity peaks associated with LiOH or Li_2CO_3 are present, which suggests that the purity of the electrolytic metal lithium is high.

The purity of the obtained electrolytic Li was evaluated via ICP-MS measurements. For comparison, commercial lithium foil with a purity >99.9 % was also measured by the same method. As shown in Fig. 5e, the purities of our deposited Li are close to the commercial Li. The mass fraction of the extracted lithium is 99.48 wt%, meeting the standard of Li-4 specified in GB/T 4369-2015. Remarkably, after extracting lithium in a solution with Mg/Li = 10, no signal of Mg was detected, indicating excellent ion selectivity of LLZTO. In the garnet lattice, Li^+ ions hop between vacancies to achieve transport; when Mg^{2+} ions, with an ionic radius of 72 p.m., very close to that of Li^+ (76 p.m.), occupy the Li^+ vacancy, the charge imbalance prevents it from hopping because the charge amounts of Li^+ and Mg^{2+} are different. In fact, the energy barrier of Li^+ is much smaller than that of impurity ions (e.g. 0.3 and 0.9 eV for Li^+ and Na^+, respectively) [42]. The high purity of the extracted Li confirms the high selectivity and high quality of the LLZTO solid electrolyte.

The comparison of the Li extraction rate between LLZTO-based devices and conventional extraction methods is shown in Table S8. Although lithium extraction materials such as MnO_2 and H_2TiO_3 as adsorbents have high adsorption capacity, their lithium extraction rates are far lower than 1 μg cm^{-2} h^{-1} [43,44]. It can be seen that the lithium extraction device based on LLZTO in this study has a very high lithium extraction rate in simulated brine, which is more than 10,000 times that of conventional adsorption methods.

The rough estimation of the overall cost of the DEEL process is shown in Supplementary Note. The overall cost consists of the costs of garnet sintering, lithium extraction and post-treatment of brine. Due to the characteristics of electrolysis, the DEEL system could be scaled up based on garnet pellets by using a parallel cell configuration (Fig. S19) or assemble the pellets into large membrane (Fig. S20). Alternatively, large garnet plates could be prepared by slip-casting process (Fig. S21) and assembled into modules (Fig. S22). If we can produce 17.5 m^2 of 500 μm thick garnet electrolyte per day for 15 days, and use them to extract lithium for 350 days, the total cost of the DEEL process is $73,105. On the product side, considering that the Li extraction rate is 126 μg cm^{-2} h^{-1}, the current efficiency is 97.71 %, and the purity of the extracted Li is 99.475 %, the amount of extracted Li in 350 days is 2700 kg, valuing $450,900 (~$167 kg^{-1}). This will make an annual profit of $377,795. Admittedly, other factors such as equipment investment, transport distances, wages, pack design may need to be further included for more realistic case.

The comparison between the DEEL process with the conventional lithium extraction method is illustrated in a radar plot in Fig. 5f based on Table S1 and some review papers [45–47]. Traditional lithium

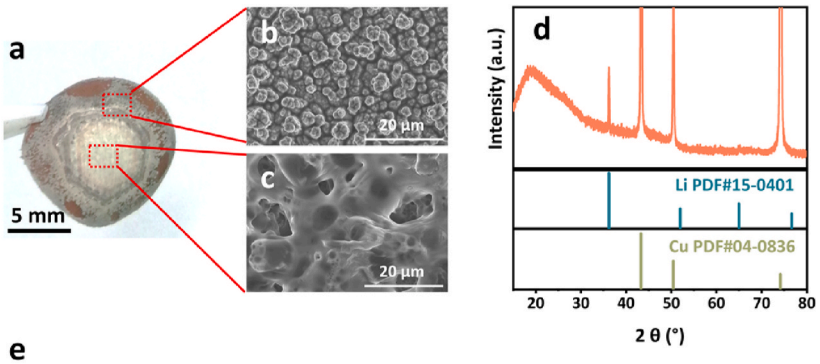

e

mg L^{-1}	C_{Li+}	C_{Mg2+}	C_{Zr4+}	C_{Ta5+}	C_{La3+}
Electrolytic Li	71.981	0.000	0.210	0.062	0.108
Li standard	72.008	0.000	0.060	0.059	0.021
Ultrapure water	0.000	0.000	0.032	0.045	0.021

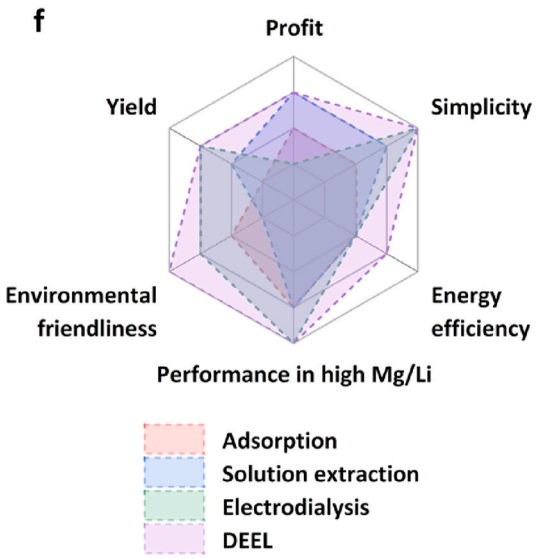

Fig. 5. | Characterization of the product of lithium metal comparison of the DEEL system with conventional methods. a, A digital photo of Cu foil deposited with Li. **b-c**, SEM images of the edge region (**b**) and the middle region (**c**). **d**, XRD patterns of Cu deposited with Li. **e**, Comparison of metal ion concentration of extracted lithium and commercial pure lithium. **f**, Comparison of the DEEL system with the three conventional methods using radar charts.

extraction methods have multiple disadvantages, such as the use of highly corrosive solvents and complex steps [45–47]. Our electrochemical lithium extraction method can be powered by clean energy sources such as solar and wind energy, without the need for additional thermal energy input during the lithium extraction process, and there are basically no by-products that cause environmental pollution. Moreover, the DEEL cell based on the sandwich-structured garnet electrolyte can directly extract lithium metal from simulated brines and natural brine. The DEEL system produces high purity lithium metal (99.48 %) at a rate of 126 μg cm^{-2} h^{-1} in a single operation. In addition, the high purity of the product lithium and the feasibility of developing electrochemical prelithiation based on the DEEL system have the potential of smooth feeding into the existing battery manufacturing supply chain.

3. Discussion

We developed a DEEL system based on LLZTO solid electrolyte as the selective membrane. Through the design of the sandwich-structured LLZTO, LZO is spontaneously formed on the LLZTO surface due to lithium volatilization during high-temperature sintering to improve water stability. The LLZTO without any polishing has high ionic conductivity (7.5×10^{-4} S cm^{-1}), low ion activation energy (0.368 eV), and low interface resistance to lithium (40 Ω cm^2). After two weeks of long-term immersion in water, the pH of deionized water only increased to about 9.8, and the corresponding concentration of dissolved lithium ions was only 0.44 ppm. The lithium extraction rate of the sandwich-structured LLZTO in simulated brine is 126 μg cm^{-2} h^{-1}. Additionally, it has good ion selectivity in simulated brine with Mg/Li = 10. The technoeconomic analysis shows that this DEEL strategy has a significantly reduced environmental impact and propitious potential profit compared with the traditional extraction methods. Moreover, the high purity of the product lithium can guarantee a smooth feeding into the existing battery manufacturing supply chain. For instance, the copper current collector deposited with the extracted lithium metal could be directly used as the anode of a lithium battery; or the DEEL process could be used as an effective pre-lithiation technique. The high efficiency, super stability, and low cost make the LLZTO-based DEEL device have great potential to extract lithium resources from salt-lake brines in the future.

4. Methods

4.1. Preparation of the sandwich-structured LLZTO

LLZTO with a garnet structure was synthesized by a modified solvent-free solid-state sintering method [30]. The preparation process is summarized in Fig. S23. Briefly, raw materials were $LiOH{\cdot}H_2O$ (AR, Shanghai Lingfeng Chemical Reagent Co., Ltd.), La_2O_3 (99.95 %, Shanghai Meiruier Chemical Technology Co., Ltd.), ZrO_2 (99.97 %, Sinopharm Chemical Reagent Co., Ltd.) and Ta_2O_5 (99.99 %, Aladdin reagent). It is named Ta5Li-4, Ta5Li0, and Ta5Li4 according to the content of Ta element (0.5) and Li element. The sample with 4 % less $LiOH{\cdot}H_2O$ added than the stoichiometric ratio is called Ta5Li-4, the sample with 4 % more than the stoichiometric ratio is called Ta5Li4, and the sample with the stoichiometric ratio is called Ta5Li0. The raw materials were weighed and dry-milled in a polyurethane milling jar at 175 r min^{-1} for 2 h. The as-mixed powders were pre-sintered at 950 °C for 6 h. The powders were dry-milled again at 175 r min^{-1} for 2 h and sieved with a 200-mesh screen. Green pellets were pressed using the 12 mm and 18 mm stainless-steel die and were put into a magnesium oxide crucible without any mother powder for secondary sintering. The temperature was raised to 1320 °C at a rising rate of 5 °C min^{-1} and furnace cooling after 10 min. Finally, the obtained LLZTO pellets were polished with SiC sandpaper of 250#, 500#, 1000#, and 2500# to prepare 40 μm-Polished and 100 μm-Polished pellets, and then were transferred to the glove box filled with argon (H_2O < 0.1 ppm and O_2 < 0.1 ppm) for storage. The thickness of the LLZTO pellets before and after polishing was measured with a micrometer caliper.

4.2. Morphology and structure characterization of the sandwich-structured LLZTO

Field emission scanning electron microscopy (SEM, RISE-MAGNA, Czech) was used to characterize the micromorphology of LLZTO ceramic pellets. The crystal phase was characterized by an X-ray diffractometer (XRD, Rigaku, 40 kV) using a Cu-Kα line with a 2θ range of 15°–60°, and the scanning speed was 5° min^{-1}. Linear scanning and surface mapping of LLZTO was performed by XRD (Bruker, D8 discover, Germany) with a 2D detector and a 2θ range of 25°–32°. Depth analysis of sandwich-structured LLZTO was performed using a high-resolution

scanning electron microscopy focused ion beam time-of-flight secondary ion mass spectrometer (TOF-SIMS, TESCAN, Czech Republic, 30 kV, 20 nA) to detect the relative intensity of lithium element signals.

The relative density of LLZTO was measured based on Archimedes' principle. The mass difference of the LLZTO pellet before and after immersion in the ethyl alcohol was used to calculate its volume. The relative density is equal to the mass before immersion divided by the product of volume and theoretical density (5.394 g cm^{-3}).

4.3. Chemical and electrochemical properties of the sandwich-structured LLZTO

The conductive silver paste (Conduction, Guangzhou) was coated on both sides of the LLZTO ceramic pellets and dried at 65 °C for 30 min to obtain Ag|LLZTO|Ag symmetric batteries. The ion conductivity of LLZTO in an Ag|LLZTO|Ag symmetric battery was measured with an impedance analyzer (Solartron 1260). The frequency range is 13 MHz to 1 Hz, and the voltage amplitude is 10 mV. The ion activation energy of LLZTO was calculated and fitted based on the Arrhenius equation by measuring different impedances in the range of 30~70 °C (take a test temperature every 10 °C). The Li|LLZTO|Li symmetric battery was prepared by hot melt infiltration. The lithium on the Ni plate was heated at 350 °C to melt, and the surface between lithium and LLZTO was continuously rubbed until wetted. The interface impedance of Li and LLZTO in Li|LLZTO|Li symmetrical battery was measured with the frequency range of 13 MHz to 0.1 Hz, and the voltage amplitude is 10 mV.

The stability of the sandwich-structured LLZTO to water and air was tested. The water stability was characterized by the degree of Li^+/H^+ exchange. The pellets were immersed in 30 mL of deionized water for two weeks, and the pH was tested with a pH meter (SX-620, Shanghai Sanxin) on the 1st, 2nd, 3rd, 4th, 5th, 6th, 7th, and 14th days respectively. To characterize the stability of LLZTO to air, the battery was placed in the atmosphere for one week, and the change of conductivity before and after storage was tested.

Li|LLZTO semi-battery is prepared by the lithium wetting method [48] and is packaged with the device shown in Fig. 1a. A Cu electrode was used as the counter electrode and reference electrode, and 1 mol L^{-1} LiCl (Yonghua, analytical pure) solution was used as the simulated brine. The constant current lithium extraction is carried out on the test system of Neware (Neware, Shenzhen, China). The current density of lithium extraction is 0.02 mA cm^{-2}, 0.04 mA cm^{-2}, 0.06 mA cm^{-2}, 0.08 mA cm^{-2}, and 0.10 mA cm^{-2}, respectively. The lithium extraction time is 1 h. In addition, the long-time constant current lithium extraction is carried out with a current density of 0.05 mA cm^{-2} and a lithium extraction time of 10 h.

80 μL of 1 M $LiPF_6$ in EC/DEC/EMC (v:v:v = 1:1:1) liquid organic electrolyte (LOE) (Nanjing Mojiesi Energy Technology Co. Ltd) was added onto the surface of LLZTO pellet, copper foil was put on top as the collector to deposit lithium, and a polypropylene diaphragm (Celgard, USA) was used to separate Cu and the LLZTO pellet. Cu electrode was used as the counter electrode and reference electrode, and LiCl solutions of different concentrations (1, 0.6, 0.33, 0.2, 0.01 mol L^{-1}) were used for lithium extraction. The current densities were 0.1 mA cm^{-2} and 0.2 mA cm^{-2}, and the time was 48 h. At the same time, 0.05 mol L^{-1} LiCl and 0.5 mol L^{-1} $MgCl_2$ (Macklin, AR, 99.5 %) + 0.05 mol L^{-1} LiCl solutions were prepared for the LLZTO ion selectivity test.

The copper foil was wrapped with Kapton adhesive to isolate air, and the structure of lithium deposition on Cu was characterized by XRD (Rigaku, 40 kV). Cu deposited with lithium was put into 15 mL ultrapure water, and inductively coupled plasma emission spectrometer (ICP, Platinum Elmer, Singapore) was used to test the lithium-ion concentration in the solution, so as to calculate the amount of lithium metal extracted; By utilizing the theoretical capacity of lithium (3860 mAh g^{-1}) to obtain the amount of lithium that can be extracted from the input capacity theoretically, the current efficiency, η, can be calculated by Equation (8).

$$m_A = C_{Li^+} \times 0.015\ \mathrm{L}$$

$$m_T = \frac{C \times 1000}{3860\ \mathrm{mAh\ g^{-1}}}$$

$$\eta = \frac{m_A}{m_T} \times 100\% \tag{8}$$

where m_A is the actual extraction amount (mg), m_T is the theoretical extraction amount (mg), C_{Li^+} is the concentration measured by ICP (mg L^{-1}), C is the input capacity (mAh), and η is the current efficiency. Commercial lithium foil (China Energy Lithium Co., Ltd, 99.9 %) with a mass of 100 m_A was weighed and put into 1500 mL of ultrapure water, and the concentration of Li^+, Mg^{2+}, Zr^{4+}, Ta^{5+}, and La^{3+} was measured by ICP.

4.4. Computation details

All density functional theory (DFT) calculations were performed using the Vienna Ab initio Simulation Package (VASP) [49] based on the projector augmented wave (PAW) [50] method. The generalized gradient approximation (GGA) with the Perdew-Burke-Ernzerhof (PBE) [51] functional was used as the exchange-correlation functional. The plane-wave energy cutoff was set to 520 eV, and a k-point density of at least 64/$Å^{-3}$, similar to those used in the Materials Project (MP) [52]. To obtain the initial structure of $Li_{52-2x}La_{24}Zr_{12}Ta_4O_{96-x}$, starting from the experimentally reported disordered structures of LLZO, and then all symmetrically distinct configurations of Li/Ta/O/Vacancy were created using the enumeration method implemented in Pymatgen code [53], Lastly, the ground state structure of $Li_{52-2x}La_{24}Zr_{12}Ta_4O_{96-x}$ was determined by ranking their DFT energies. Temperature-dependent Gibbs free energies were calculated by using the Phonopy package [54].

CRediT authorship contribution statement

Nan Zhang: Writing – original draft, Visualization, Validation, Methodology, Investigation, Formal analysis, Data curation. **Hongpeng Zheng:** Visualization, Validation, Methodology, Investigation, Formal analysis, Data curation, Conceptualization. **Guoyao Li:** Validation, Methodology, Investigation, Formal analysis. **Cheng Ouyang:** Visualization, Methodology, Investigation. **Yu Yang:** Visualization, Software, Methodology. **Hong Zhu:** Software, Resources, Formal analysis. **Rongzi Zhang:** Resources, Project administration. **Haidong Sun:** Resources, Project administration. **Chenglan Zhang:** Resources, Project administration. **Hezhou Liu:** Resources, Project administration. **Huanan Duan:** Writing – review & editing, Supervision, Resources, Methodology, Funding acquisition, Formal analysis, Conceptualization.

Declaration of competing interest

The authors declare the following financial interests/personal relationships which may be considered as potential competing interests: R. Z., H.S., and C.Z. are employees of QingHai Salt Lake industry Co., Ltd., which is trying to commercialize relevant technology. The remaining authors declare no competing interests.

Acknowledgments

This work was supported by Key R&D and Transformation Plan Projects of QingHai Salt Lake Industry Co., Ltd. (10000000-22-ZC0609-0011). H.D. acknowledges support from the National Natural Science Foundation of China under grant no. 51972211.

Appendix A. Supplementary data

Supplementary data to this article can be found online at https://doi.

org/10.1016/j.jpowsour.2024.236119.

Data availability

Data will be made available on request.

References

[1] L. Kavanagh, J. Keohane, G. Garcia Cabellos, A. Lloyd, J. Cleary, Global lithium sources—industrial use and future in the electric vehicle industry: a review, Resources 7 (2018) 57.

[2] G. Liu, Z. Zhao, A. Ghahreman, Novel approaches for lithium extraction from salt-lake brines: a review, Hydrometallurgy 187 (2019) 81–100, https://doi.org/10.1016/j.hydromet.2019.05.005.

[3] Y. Zhang, Y. Hu, N. Sun, R. Liu, Z. Wang, L. Wang, W. Sun, Systematic review of feldspar beneficiation and its comprehensive application, Miner. Eng. 128 (2018) 141–152, https://doi.org/10.1016/j.mineng.2018.08.043.

[4] H. Vikström, S. Davidsson, M. Höök, Lithium availability and future production outlooks, Appl. Energy 110 (2013) 252–266, https://doi.org/10.1016/j.apenergy.2013.04.005.

[5] F. Naseri, Z. Kazemi, F. Shabaninia, Electric and plug-in hybrid electric vehicles. Conference of the, IEEE Industrial Electronics Society, 2013.

[6] Y. Xiong, J. Zhou, P. Lu, J. Yin, Y. Wang, Z. Fan, Electrochemical lithium extraction from aqueous sources, Matter 5 (6) (2022) 1760–1791, https://doi.org/10.1016/j.matt.2022.04.034.

[7] P. Loganathan, G. Naidu, S. Vigneswaran, Mining valuable minerals from seawater: a critical review, Environ. Sci. J. Integr. Environ. Res.: Water Res. Techno. 3 (1) (2017) 37–53, https://doi.org/10.1039/C6EW00268D.

[8] X. Li, Y. Mo, W. Qing, S. Shao, C.Y. Tang, J. Li, Membrane-based technologies for lithium recovery from water lithium resources: a review, J. Membr. Sci. 591 (2019) 117317, https://doi.org/10.1016/j.memsci.2019.117317.

[9] B.K. Pramanik, L.D. Nghiem, F.I. Hai, Extraction of strategically important elements from brines: constraints and opportunities, Water Res. 168 (2020) 115149, https://doi.org/10.1016/j.watres.2019.115149.

[10] J. Jandová, P. Dvořák, H.N. Vu, Processing of zinnwaldite waste to obtain Li2CO3, Hydrometallurgy 103 (1) (2010) 12–18, https://doi.org/10.1016/j.hydromet.2010.02.010.

[11] L. Xing, J. Song, Z. Li, J. Liu, T. Huang, P. Dou, Y. Chen, X.-M. Li, T. He, Solvent stable nanoporous poly (ethylene-co-vinyl alcohol) barrier membranes for liquid-liquid extraction of lithium from a salt lake brine, J. Membr. Sci. 520 (2016) 596–606, https://doi.org/10.1016/j.memsci.2016.08.027.

[12] Y. Yang, S. Xu, Y. He, Lithium recycling and cathode material regeneration from acid leach liquor of spent lithium-ion battery via facile co-extraction and co-precipitation processes, Waste Manag. 64 (2017) 219–227, https://doi.org/10.1016/j.wasman.2017.03.018.

[13] J.-L. Xiao, S.-Y. Sun, X. Song, P. Li, J.-G. Yu, Lithium ion recovery from brine using granulated polyacrylamide–MnO2 ion-sieve, Chem. Eng. J. 279 (2015) 659–666, https://doi.org/10.1016/j.cej.2015.05.075.

[14] B. Swain, Recovery and recycling of lithium: a review, Separ. Purif. Technol. 172 (2017) 388–403, https://doi.org/10.1016/j.seppur.2016.08.031.

[15] L. Yang, Y. Tu, H. Li, W. Zhan, H. Hu, Y. Wei, C. Chen, K. Liu, P. Shao, M. Li, G. Yang, X. Luo, Fluorine-rich supramolecular nano-container crosslinked hydrogel for lithium extraction with super-high capacity and extreme selectivity, Angew. Chem. Int. Ed. 62 (38) (2023) e202308702, https://doi.org/10.1002/anie.202308702.

[16] X.-R. Pan, W.-W. Li, L. Huang, H.-Q. Liu, Y.-K. Wang, Y.-K. Geng, P. Kwan-Sing Lam, H.-Q. Yu, Recovery of high-concentration volatile fatty acids from wastewater using an acidogenesis-electrodialysis integrated system, Bioresour. Technol. 260 (2018) 61–67, https://doi.org/10.1016/j.biortech.2018.03.083.

[17] X.-Y. Nie, S.-Y. Sun, Z. Sun, X. Song, J.-G. Yu, Ion-fractionation of lithium ions from magnesium ions by electrodialysis using monovalent selective ion-exchange membranes, Desalination 403 (2017) 128–135, https://doi.org/10.1016/j.desal.2016.05.010.

[18] L. Yang, Z. Gao, T. Liu, M. Huang, G. Liu, Y. Feng, P. Shao, X. Luo, Direct electrochemical leaching method for high-purity lithium recovery from spent lithium batteries, Environ. Sci. Technol. 57 (11) (2023) 4591–4597, https://doi.org/10.1021/acs.est.3c00287.

[19] Q. Xia, Z. Deng, S. Sun, W. Zhao, J. Ding, B. Xi, G. Gao, C. Wang, Solar-enhanced lithium extraction with self-sustaining water recycling from salt-lake brines, Proc. Natl. Acad. Sci. USA 121 (23) (2024) e2400159121, https://doi.org/10.1073/pnas.2400159121.

[20] Y. Song, S. Fang, N. Xu, M. Wang, S. Chen, J. Chen, B. Mi, J. Zhu, Solar transpiration–powered lithium extraction and storage, Science 385 (6716) (2024) 1444–1449, https://doi.org/10.1126/science.adm7034.

[21] B. Tansel, Significance of thermodynamic and physical characteristics on permeation of ions during membrane separation: hydrated radius, hydration free energy and viscous effects, Separ. Purif. Technol. 86 (2012) 119–126, https://doi.org/10.1016/j.seppur.2011.10.033.

[22] S. Yang, F. Zhang, H. Ding, P. He, H. Zhou, Lithium metal extraction from seawater, Joule 2 (9) (2018) 1648–1651, https://doi.org/10.1016/j.joule.2018.07.006.

[23] X. Zhao, H. Zhang, Y. Yuan, Y. Ren, N. Wang, Ultra-fast and stable extraction of Li metal from seawater, Chem. Commun. 56 (10) (2020) 1577–1580, https://doi.org/10.1039/C9CC08927F.

[24] H. Zhang, Y. Ren, X. Wu, N. Wang, An interface-modified solid-state electrochemical device for lithium extraction from seawater, J. Power Sources 482 (2021) 228938, https://doi.org/10.1016/j.jpowsour.2020.228938.

[25] J. Xu, Y. Jin, K. Liu, N. Lyu, Z. Zhang, B. Sun, Q. Jin, H. Lu, H. Tian, X. Guo, D. Shanmukaraj, H. Wu, M. Li, M. Armand, G. Wang, A green and sustainable strategy toward lithium resources recycling from spent batteries, Sci. Adv. 8 (40) (2022) eabq7948.

[26] C.-Z. Zhao, P.-Y. Chen, R. Zhang, X. Chen, B.-Q. Li, X.-Q. Zhang, X.-B. Cheng, Q. Zhang, An ion redistributor for dendrite-free lithium metal anodes, Sci. Adv. 4 (11) (2018) eaat3446.

[27] W. Feng, J. Hu, G. Qian, Z. Xu, G. Zan, Y. Liu, F. Wang, C. Wang, Y. Xia, Stabilization of garnet/Li interphase by diluting the electronic conductor, Sci. Adv. 8 (42) (2022) eadd8972.

[28] Y. Shimonishi, A. Toda, T. Zhang, A. Hirano, N. Imanishi, O. Yamamoto, Y. Takeda, Synthesis of garnet-type Li7−xLa3Zr2O12−1/2x and its stability in aqueous solutions, Solid State Ionics 183 (1) (2011) 48–53, https://doi.org/10.1016/j.ssi.2010.12.010.

[29] W. Xia, B. Xu, H. Duan, X. Tang, Y. Guo, H. Kang, H. Li, H. Liu, Reaction mechanisms of lithium garnet pellets in ambient air: the effect of humidity and CO2, J. Am. Ceram. Soc. 100 (7) (2017) 2832–2839, https://doi.org/10.1111/jace.14865.

[30] H. Zheng, G. Li, J. Liu, S. Wu, X. Zhang, Y. Wu, H. Zhu, X. Huang, H. Liu, H. Duan, A rational design of garnet-type Li7La3Zr2O12 with ultrahigh moisture stability, Energy Storage Mater. 49 (2022) 278–290, https://doi.org/10.1016/j.ensm.2022.04.027.

[31] K. Lee, E. Kazyak, M.J. Wang, N.P. Dasgupta, J. Sakamoto, Analyzing void formation and rewetting of thin in situ-formed Li anodes on LLZO, Joule 6 (11) (2022) 2547–2565, https://doi.org/10.1016/j.joule.2022.09.009.

[32] M. Zheng, X. Liu, Hydrochemistry of salt lakes of the qinghai-tibet plateau, China, Aquat. Geochem. 15 (1) (2009) 293–320, https://doi.org/10.1007/s10498-008-9055-y.

[33] T. Zhang, W. Zheng, Q. Wang, Z. Wu, Z. Wang, Designed strategies of nanofiltration technology for Mg2+/Li+ separation from salt-lake brine: a comprehensive review, Desalination 546 (2023) 116205, https://doi.org/10.1016/j.desal.2022.116205.

[34] L. Cheng, W. Chen, M. Kunz, K. Persson, N. Tamura, G. Chen, M. Doeff, Effect of surface microstructure on electrochemical performance of garnet solid electrolytes, ACS Appl. Mater. Interfaces 7 (3) (2015) 2073–2081, https://doi.org/10.1021/am508111r.

[35] R.H. Brugge, A.K.O. Hekselman, A. Cavallaro, F.M. Pesci, R.J. Chater, J.A. Kilner, A. Aguadero, Garnet electrolytes for solid state batteries: visualization of moisture-induced chemical degradation and revealing its impact on the Li-ion dynamics, Chem. Mater. 30 (11) (2018) 3704–3713, https://doi.org/10.1021/acs.chemmater.8b00486.

[36] W. Zhang, Q. Wu, J. Huang, L. Fan, Z. Shen, Y. He, Q. Feng, G. Zhu, Y. Lu, Colossal granular lithium deposits enabled by the grain-coarsening effect for high-efficiency lithium metal full batteries, Adv. Mater. 32 (24) (2020) 2001740, https://doi.org/10.1002/adma.202001740.

[37] X. Wang, Y. Hou, Y. Zhu, Y. Wu, R. Holze, An aqueous rechargeable lithium battery using coated Li metal as anode, Sci. Rep. 3 (1) (2013) 1401, https://doi.org/10.1038/srep01401.

[38] J. Ying, M. Luo, Y. Jin, J. Yu, Selective separation of lithium from high Mg/Li ratio brine using single-stage and multi-stage selective electrodialysis processes, Desalination 492 (2020) 114621, https://doi.org/10.1016/j.desal.2020.114621.

[39] G. Liu, Z. Zhao, L. He, Highly selective lithium recovery from high Mg/Li ratio brines, Desalination 474 (2020) 114185, https://doi.org/10.1016/j.desal.2019.114185.

[40] C. Yang, H. Ma, R. Yuan, K. Wang, K. Liu, Y. Long, F. Xu, L. Li, H. Zhang, Y. Zhang, X. Li, H. Wu, Roll-to-roll prelithiation of lithium-ion battery anodes by transfer printing, Nat. Energy 8 (7) (2023) 703–713, https://doi.org/10.1038/s41560-023-01272-1.

[41] Y. Wang, J. Tan, Z. Li, L. Ma, Z. Liu, M. Ye, J. Shen, Recent progress on enhancing the Lithiophilicity of hosts for dendrite-free lithium metal batteries, Energy Storage Mater. 53 (2022) 156–182, https://doi.org/10.1016/j.ensm.2022.09.006.

[42] H. Zhang, J. Lang, K. Liu, Y. Jin, K. Wang, Y. Wu, S. Shi, L. Wang, H. Xu, X. He, H. Wu, High ion-selectivity of garnet solid electrolyte enabling separation of metallic lithium, Energy Environ. Mater. (n/a) (2022) e12425, https://doi.org/10.1002/eem2.12425.

[43] S. Zandevakili, M. Ranjbar, M. Ehteshamzadeh, Recovery of lithium from Urmia Lake by a nanostructure MnO2 ion sieve, Hydrometallurgy 149 (2014) 148–152, https://doi.org/10.1016/j.hydromet.2014.08.004.

[44] S. Wei, Y. Wei, T. Chen, C. Liu, Y. Tang, Porous lithium ion sieves nanofibers: general synthesis strategy and highly selective recovery of lithium from brine water, Chem. Eng. J. 379 (2020) 122407, https://doi.org/10.1016/j.cej.2019.122407.

[45] R. Krishnan, G. Gopan, A comprehensive review of lithium extraction: from historical perspectives to emerging technologies, storage, and environmental considerations, Clean Eng. Techno. 20 (2024) 100749, https://doi.org/10.1016/j.clet.2024.100749.

[46] J.F. Song, L.D. Nghiem, X.-M. Li, T. He, Lithium extraction from Chinese salt-lake brines: opportunities, challenges, and future outlook, Environ. Sci. J. Integr. Environ. Res.: Water Res. Techno. 3 (4) (2017) 593–597, https://doi.org/10.1039/C7EW00020K.

[47] A.C. Alera, J.P. Benitez, R.J. Fernandez, C.K. Pascual, F. Policarpio, E.C. Lopez, Recent advances in lithium extraction, Eng. Proce. 67 (2024) 52.

[48] H. Zheng, G. Li, R. Ouyang, Y. Han, H. Zhu, Y. Wu, X. Huang, H. Liu, H. Duan, Origin of lithiophilicity of lithium garnets: compositing or cleaning? Adv. Funct. Mater. 32 (41) (2022) 2205778 https://doi.org/10.1002/adfm.202205778.
[49] G. Kresse, J. Furthmüller, Efficient iterative schemes for ab initio total-energy calculations using a plane-wave basis set, Phys. Rev. B 54 (16) (1996) 11169–11186, https://doi.org/10.1103/PhysRevB.54.11169.
[50] P.E. Blöchl, Projector augmented-wave method, Phys. Rev. B 50 (24) (1994) 17953–17979, https://doi.org/10.1103/PhysRevB.50.17953.
[51] J.P. Perdew, K. Burke, M. Ernzerhof, Generalized gradient approximation made simple, Phys. Rev. Lett. 77 (18) (1996) 3865–3868, https://doi.org/10.1103/PhysRevLett.77.3865.
[52] A. Jain, S.P. Ong, G. Hautier, W. Chen, W.D. Richards, S. Dacek, S. Cholia, D. Gunter, D. Skinner, G. Ceder, K.A. Persson, Commentary: the Materials Project: a materials genome approach to accelerating materials innovation, Apl. Mater. 1 (1) (2013), https://doi.org/10.1063/1.4812323.
[53] S.P. Ong, W.D. Richards, A. Jain, G. Hautier, M. Kocher, S. Cholia, D. Gunter, V. L. Chevrier, K.A. Persson, G. Ceder, Python Materials Genomics (pymatgen): a robust, open-source python library for materials analysis, Comput. Mater. Sci. 68 (2013) 314–319, https://doi.org/10.1016/j.commatsci.2012.10.028.
[54] A. Togo, I. Tanaka, First principles phonon calculations in materials science, Scripta Mater. 108 (2015) 1–5, https://doi.org/10.1016/j.scriptamat.2015.07.021.